

# Phosphorescent platinum(II) complexes containing different $\beta$ -diketonate ligands: synthesis, tunable excited-state properties, and their application in bioimaging†

Xin Mou,<sup>a</sup> Yongquan Wu,<sup>b</sup> Shujuan Liu,<sup>a</sup> Mei Shi,<sup>\*b</sup> Xiangmei Liu,<sup>a</sup> Chuanming Wang,<sup>c</sup> Shi Sun,<sup>a</sup> Qiang Zhao,<sup>\*a</sup> Xinhui Zhou<sup>a</sup> and Wei Huang<sup>\*a</sup>

Received 17th February 2011, Accepted 24th June 2011

DOI: 10.1039/c1jm10718f

A series of square-planar Pt(II) complexes [Pt(C<sup>N</sup>)(O<sup>O</sup>)] (**1–5**) (C<sup>N</sup> = 2-phenylpyridine, O<sup>O</sup> denotes a series of  $\beta$ -diketonate ligands) is reported. Detailed studies of theoretical calculations, electrochemical and photophysical properties have shown that their excited states can be attributed to the mixing of <sup>3</sup>MLCT, <sup>3</sup>LLCT and <sup>3</sup>LC/<sup>3</sup>ILCT transitions. For **1**, the excited state is dominated by the C<sup>N</sup> ligand. The excited states of complexes **2–5**, however, are dominated by O<sup>O</sup> ligands. Through variation of the  $\beta$ -diketonate ligands, the emission colors of **1–5** can be tuned from blue-green to yellow. Further investigations have revealed that the emission of **4** in the solid state can be attributed to the <sup>3</sup>MLCT and <sup>3</sup>LLL'CT transitions, which has been confirmed by X-ray diffraction studies as well as theoretical calculations. Moreover, exclusive staining of cytoplasm and low cytotoxicity have been observed for **1–4**, which makes them promising candidates as phosphorescent probes for bioimaging.

## Introduction

Phosphorescent cyclometalated Pt(II) complexes, due to their unique spectroscopic properties, have attracted a great deal of attention in recent years.<sup>1–7</sup> Most of the reported cyclometalated Pt(II) complexes are heteroleptic and the platinum atom is coordinated by one cyclometalated C<sup>N</sup> ligand and one ancillary ligand. Their photophysical properties are usually determined by the cyclometalated C<sup>N</sup> ligand and can be tuned significantly by changing the degree of conjugation of this ligand.<sup>8</sup> In addition to the C<sup>N</sup> ligand, the nature of the ancillary ligand may also have a profound effect on the lowest excited state of such a complex.<sup>9</sup>  $\beta$ -Diketonates (O<sup>O</sup> ligands) are an important class of ancillary ligands. Pt(II) complexes containing  $\beta$ -diketonate ligands exhibit intriguing emissive properties and have attracted increasing interest in recent years.<sup>6a,10</sup> However, most reported studies have focused on Pt(II) complexes containing  $\beta$ -diketonate ligands with high triplet-state energy levels, such as acetylacetonate (acac) and

2,2,6,6-tetramethyl-3,5-heptanedionate (dpm).<sup>6a,8a</sup> For these, the  $\beta$ -diketonate ligands have little influence on the photophysical properties. To date, little effort has been devoted to investigating the detailed influence of  $\beta$ -diketonate ligands with low triplet-state energy levels on the photophysical and excited-state properties of Pt(II) complexes.<sup>11</sup> If the photophysical and excited-state properties of Pt(II) complexes could be significantly tuned through the modification of  $\beta$ -diketonate ligands, it would be very useful for the molecular design of Pt(II) complexes.

Besides the pure research concerning the relationship between the phosphorescence emission and chemical structure of Pt(II) complexes, increasing interest is being directed towards the application of such systems in several optical and electronic fields, such as organic light-emitting diodes,<sup>4</sup> singlet oxygen sensitizers,<sup>5</sup> chemosensors,<sup>6</sup> and bioprobes,<sup>7</sup> *etc.* Recently, the application of phosphorescent Pt(II) complexes as bioimaging probes has emerged as a new and active research field,<sup>12</sup> due to their advantageous photophysical properties in bioimaging, such as high luminescence efficiency, significant Stokes shifts, tunable excitation and emission wavelengths over the whole visible range, and relatively long emission lifetimes. In particular, a long phosphorescence lifetime could eliminate interference from short-lifetime autofluorescence in biological samples by using a time-resolved luminescence technique.<sup>13</sup> To date, several examples have reported the use of Pt(II) complexes with N<sup>C</sup>C<sup>N</sup>,<sup>13</sup> N<sup>N</sup>C<sup>N</sup>,<sup>14</sup> and porphyrin ligands<sup>15</sup> as bioimaging materials. For example, Williams *et al.* reported the first example of time-resolved imaging based on Pt(II) complexes with N<sup>C</sup>C<sup>N</sup> ligands, utilizing their long emission lifetimes.<sup>13</sup> Che *et al.*

<sup>a</sup>Key Laboratory for Organic Electronics & Information Displays (KLOEID), Institute of Advanced Materials (IAM), Nanjing University of Posts and Telecommunications, 210046 Nanjing, China. E-mail: wei-huang@njupt.edu.cn; iamqzhao@njupt.edu.cn; Fax: +86-25-85866396

<sup>b</sup>Department of Chemistry, Fudan University, 200433 Shanghai, China. E-mail: shimei@fudan.edu.cn; Fax: +86-21-55664185

<sup>c</sup>Shanghai Research Institute of Petrochemical Technology, SINOPEC, Shanghai, 201208, China

† Electronic supplementary information (ESI) available: Table S1–S5, Fig S1–S8. CCDC reference number 758055. For ESI and crystallographic data in CIF or other electronic format see DOI: 10.1039/c1jm10718f

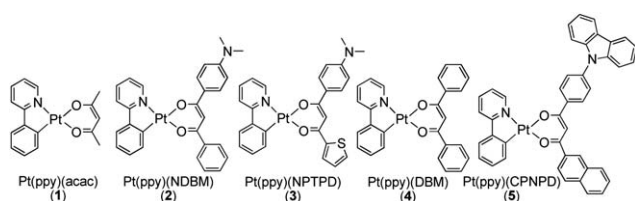
realized the staining of intact cellular proteins by Pt(II) complexes with N<sup>N</sup>^C ligands.<sup>14a</sup> Lam *et al.* reported a two-photon active Pt(II) complex with an N<sup>N</sup>^C ligand for cytoplasm staining.<sup>14b</sup> These examples showed Pt(II) complexes to be a class of excellent bioimaging materials. However, Pt(II) complexes containing  $\beta$ -diketonate ligands, as another class of important phosphorescent dyes, have hitherto been ignored in bioimaging.

For the present study, we chose a series of  $\beta$ -diketonates with relatively low triplet-state energy levels as O<sup>^O</sup> ligands to synthesize several new cyclometalated Pt(II) complexes, [Pt(ppy)(NDBM)] (2), [Pt(ppy)(NPTPD)] (3), [Pt(ppy)(DBM)] (4), and [Pt(ppy)(CPNPD)] (5) (Scheme 1, where ppy = 2-phenylpyridine, NDBM = 4-(dimethylamino)-dibenzoylmethane, NPTPD = 1-(4-(dimethylamino)phenyl)-3-(thiophen-2-yl)propane-1,3-dione, DBM = dibenzoylmethane and CPNPD = 1-(4-(9H-carbazol-9-yl)phenyl)-3-(naphthalen-2-yl)propane-1,3-dione) and studied their photophysical and electrochemical properties in solution. For comparison, the well-known complex [Pt(ppy)(acac)] (1) (see Scheme 1, where acac = acetylacetonate) was also investigated. Interestingly, studies of the photophysical and electrochemical properties of Pt(II) complexes 1–5 in solution have shown that their photophysical and excited-state properties can be significantly tuned through changing the  $\beta$ -diketonate ligands. In addition, the relationship between the structure and emission properties of [Pt(ppy)(DBM)] in the solid state has also been investigated by single-crystal X-ray diffraction analysis as well as density functional theory (DFT) calculations. Furthermore, Pt(II) complexes 1–4 have been investigated for use as multicolor phosphorescent dyes with tunable emission from blue-green to yellow for staining the cytoplasm of living cells.

## Experimental

### Equipment

NMR spectra were recorded on a Bruker Ultra Shield Plus 400 MHz NMR instruments (<sup>1</sup>H, 400 MHz; <sup>13</sup>C, 100 MHz). Mass spectra were obtained on a Bruker autoflex MALDI-TOF/TOF mass spectrometer or LCQ Fleet ESI mass spectrometer. The elemental analyses were performed on a VarioEL III O-Element Analyzer system. Electrochemical measurements were performed with a CHI660E. The UV-visible absorption spectra were recorded on a Shimadzu UV-3600 UV-VIS-NIR spectrophotometer. Photoluminescent spectra were measured using a RF-5301PC spectrofluorophotometer. Quantum efficiency measurements were carried out at room temperature in a dichloromethane solution. Before spectra were measured, the solution was degassed by several freeze-pump-thaw cycles using a diffusion pump. Ir(ppy)<sub>3</sub> (*fac*-[Ir(ppy)<sub>3</sub>]: *fac*-tris(2-phenylpyridine) iridium) ( $\Phi = 0.40$  at 360 nm) was used as a reference.<sup>16</sup>



**Scheme 1** Chemical structures of the Pt(II) complexes 1–5.

The equation  $\Phi_s = \Phi_r(\eta_s^2 A_r I_s)/(\eta_r^2 A_s I_r)$  was used to calculate quantum yields, where  $\Phi_s$  is the quantum yield of the sample,  $\Phi_r$  is the quantum yield of the reference,  $\eta$  is the refractive index of the solvent,  $A_s$  and  $A_r$  are the absorbances of the sample and the reference at the wavelength of excitation, and  $I_s$  and  $I_r$  are the integrated areas of the emission bands.<sup>16,17</sup>

### Theoretical calculations

Density functional theory calculations were employed to investigate the nature of the low-lying excited electronic states in these complexes. The ground state and triplet state were optimized at the B3LYP and unrestricted B3LYP (UB3LYP) levels, respectively. On the basis of ground and triplet state optimization, the time-dependent density functional theory (TDDFT) approach was applied to study the excited-state properties of the complexes in solution. The solvent (CH<sub>2</sub>Cl<sub>2</sub>) effect was simulated using the polarizable continuum model (PCM) in which the solvent cavity is regarded as a union of interlocking atomic spheres. The LANL2DZ and 6-31G(d) basis sets were employed for the Pt(II) atom and the other atoms, respectively. All these calculations were accomplished by using the Gaussian 03 software package.<sup>18</sup> The molecular structure and crystal structure of complex 4 were optimized using DFT calculations with the double numerical basis set with polarization functions (DNP) and the generalized gradient corrected Perdew–Burke–Ernzerhof (GGA-PBE) functional implemented in the DMol3 package.<sup>19</sup> The real space cutoff distance was 3.6 Å. The core electrons of all atoms were represented by semi-core pseudopotentials (DSPP).<sup>20</sup> The Brillouin zone was sampled only by Gamma-point. Geometry optimization was performed using the Broyden–Fletcher–Goldfarb–Shanno algorithm with a convergence criterion of  $5 \times 10^{-3}$  hartree on the displacement and  $4 \times 10^{-3}$  hartree on the gradient and  $1 \times 10^{-4}$  hartree on the total energy.

### Electrochemical measurements

All measurements were carried out in a one-compartment cell under N<sub>2</sub> gas, equipped with a glassy-carbon working electrode, a platinum wire counter electrode, and an Ag/Ag<sup>+</sup> reference electrode. Measurements of oxidation and reduction were undertaken in anhydrous solutions of CH<sub>2</sub>Cl<sub>2</sub> and DMF, respectively, containing 0.10 mol L<sup>-1</sup> tetrabutylammonium hexafluorophosphate (Bu<sub>4</sub>NPF<sub>6</sub>) as the supporting electrolyte. The ferrocene/ferrocenium couple was added and used as the internal standard. The scan rate was 50 mV s<sup>-1</sup>.

### X-Ray crystallography analysis

The crystal structure of complex 4 was determined on a Siemens (Bruker) SMART CCD diffractometer using monochromated Mo-K $\alpha$  radiation ( $\lambda = 0.71073$  Å) at room temperature. The structure was solved by direct methods and refined by full-matrix least-squares on  $F^2$  using the program SHELXL-97.<sup>21</sup> All non-hydrogen atoms were refined anisotropically. Hydrogen atoms were placed in calculated position and refined as riding atoms with a uniform value of Uiso. For the full-matrix least-squares refinements [ $I > 2\sigma(I)$ ], the unweighted and weighted agreement factors of  $R_1 = \Sigma||F_o| - |F_c||/\Sigma|F_o|$  and  $wR_2 = [\Sigma w(F_o^2 - F_c^2)^2/\Sigma w(F_o^2)]^{1/2}$  were used. CCDC reference number for 4 is 758055.†

## Materials

All reagents and chemicals were purchased from commercial sources and used without further purification. 2-Phenylpyridine, Hacac and HDBM were purchased from Aldrich Chemical Co. All complexes were synthesized according to the previous report.<sup>1b,11</sup> All other ligands and materials were purchased from either Aldrich Chemical Co. or Acros.

## Synthesis of diketonate ligands

All diketonate ligands were synthesized according to the same procedure (see Scheme 2). Herein, only the synthesis of ligand HNDBM was described in detail.

**HNDBM.** This compound was synthesized according to a modified procedure reported in the previous literature.<sup>22</sup> A mixture of a sodium hydride in oil dispersion (60%, 0.53 g, 22 mmol) and ethyl *p*-(dimethylamino)benzoate (1.93 g, 10 mmol) in 30 mL of dry THF was heated to 60 °C. Acetophenone (1.20 g, 10 mmol) in 15 mL of dry THF was added dropwise to the mixture. After the reaction temperature was kept at 60 °C for 1 day, the mixture was poured into water and then neutralized with hydrochloric acid. The resulting precipitate was recrystallized from ethanol to give green-yellow crystals in 36% yield. <sup>1</sup>H NMR (400 MHz, CDCl<sub>3</sub>) δ: 17.20 (s, 1H; OH), 7.91–7.97 (m, 4H; ArH), 7.45–7.52 (m, 3H; ArH), 6.77 (s, 1H; C–CH=), 6.71 (s, 1H; ArH), 6.68 (s, 1H; ArH), 3.06 (s, 6H; CH<sub>3</sub>); <sup>13</sup>C NMR (100 MHz, CDCl<sub>3</sub>) δ: 40.04, 91.76, 111.05, 122.68, 126.82, 128.56, 129.33, 131.70, 135.95, 153.35, 182.20, 186.89. Anal. calcd for C<sub>17</sub>H<sub>17</sub>NO<sub>2</sub>: C, 76.38; H, 6.41; N, 5.24. Found: C, 76.11; H, 6.73; N, 5.59.

**HNPTPD.** 32% yield. <sup>1</sup>H NMR (400 MHz, CDCl<sub>3</sub>) δ: 16.78 (s, 1H; OH), 7.88 (t, *J* = 2.35 Hz, 2H; ArH), 7.86 (t, *J* = 2.51 Hz, 1H; ArH), 7.75 (dd, *J* = 1.06, 1.07 Hz, 1H; ArH), 7.57 (dd, *J* = 1.04, 1.11 Hz, 1H; ArH), 7.15 (m, 1H; ArH), 6.72 (t, *J* = 2.50 Hz, 1H; ArH), 6.69 (t, *J* = 2.51 Hz, 1H; ArH), 6.60 (s, 1H; C–CH=), 3.08 (s, 6H; CH<sub>3</sub>). <sup>13</sup>C NMR (100 MHz, CDCl<sub>3</sub>) δ: 40.08, 91.10, 111.12, 128.09, 128.93, 129.13, 131.17, 131.44, 134.55, 153.24, 180.11, 182.67. Anal. calcd for C<sub>15</sub>H<sub>15</sub>NO<sub>2</sub>S: C, 65.91; H, 5.53; N, 5.12. Found: C, 65.63; H, 5.41; N, 5.29.

**HCPNPD.** 39% yield. <sup>1</sup>H NMR (400 MHz, CDCl<sub>3</sub>) δ: 17.06 (s, 1H; OH), 8.60 (s, 1H; ArH), 8.28 (d, *J* = 8.49 Hz, 2H; ArH), 8.17 (m, 2H; ArH), 8.07 (d, *J* = 8.65 Hz, 1H; ArH), 8.01 (d, *J* = 7.77

Hz, 1H; ArH), 7.96 (d, *J* = 8.64 Hz, 1H; ArH), 7.91 (d, *J* = 7.51 Hz, 1H; ArH), 7.75 (d, *J* = 8.63 Hz, 2H; ArH), 7.60 (t, *J* = 7.48 Hz, 2H; ArH), 7.52 (d, *J* = 8.21 Hz, 2H; ArH), 7.46 (t, *J* = 7.80 Hz, 2H; ArH), 7.35 (t, *J* = 7.36 Hz, 2H; ArH), 7.10 (s, 1H; C–CH=); <sup>13</sup>C NMR (100 MHz, CDCl<sub>3</sub>) δ: 93.56, 109.84, 120.51, 120.61, 123.28, 123.86, 126.25, 126.68, 126.91, 127.85, 128.30, 128.50, 128.61, 128.97, 129.45, 132.69, 132.80, 134.13, 135.43, 140.31, 141.59, 184.65, 185.69. Anal. calcd for C<sub>31</sub>H<sub>21</sub>NO<sub>2</sub>: C, 84.72; H, 4.82; N, 3.19. Found: C, 84.56; H, 4.43; N, 3.01.

## Synthesis of complexes [Pt(C<sup>^</sup>N)(O<sup>^</sup>O)]

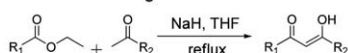
All Pt(II) complexes Pt(C<sup>^</sup>N)(O<sup>^</sup>O) were synthesized according to the same procedure. Herein, only the synthesis of complex Pt(ppy)(NDBM) (**2**) is described in detail.

**[Pt(ppy)(NDBM)] (**2**).** The Pt(II) chlorobridged dimer [Pt(ppy)Cl]<sub>2</sub> was prepared according to a literature procedure.<sup>1b,d</sup> A solution of [Pt(ppy)Cl]<sub>2</sub> (260 mg, 0.338 mmol), 4-(dimethylamino)-dibenzoylmethane (271 mg, 1.014 mmol) and 10 eq. of Na<sub>2</sub>CO<sub>3</sub> in 2-ethoxyethanol (30 ml) was heated to reflux for 16 h. Then the reaction mixture was concentrated under reduced pressure. An excess of water was added gradually to give orange-green precipitate of crude product that was subsequently filtered and washed with water. The obtained crude product was purified by silica gel column chromatography using dichloromethane as the eluent to give 0.12 g of the product in 29% yield. <sup>1</sup>H NMR (400 MHz, CDCl<sub>3</sub>, 298 K) δ: 9.21 (dd, *J* = 5.59, 5.66 Hz, 1H; pyridine-H), 8.02–8.09 (m, 4H; ArH), 7.80–7.86 (m, 2H; ArH), 7.66 (d, *J* = 8.2 Hz, 1H; ArH), 7.47–7.54 (m, 4H; ArH), 7.29 (d, *J* = 7.2 Hz, 1H; ArH), 7.11–7.20 (m, 2H; ArH), 6.73–6.75 (m, 2H; ArH), 6.76 (s, 1H; C–CH=), 3.07 (s, 3H; CH<sub>3</sub>), 3.06 (s, 3H; CH<sub>3</sub>); <sup>13</sup>C NMR (100 MHz, CDCl<sub>3</sub>) δ: 40.10, 97.58, 111.22, 118.59, 121.51, 123.21, 123.85, 126.67, 127.06, 127.18, 128.09, 128.69, 128.74, 129.42, 129.80, 130.87, 131.05, 138.41, 139.00, 139.34, 140.27, 144.90, 147.34, 152.23, 168.51, 178.96, 180.02. Anal. calcd for C<sub>28</sub>H<sub>24</sub>N<sub>2</sub>O<sub>2</sub>Pt: C, 54.63; H, 3.93; N, 4.55. Found: C, 54.31; H, 3.62; N, 4.75. MS (MALDI-TOF/TOF) *m/z*: 615.473 ([M]<sup>+</sup>, calcd for C<sub>28</sub>H<sub>24</sub>N<sub>2</sub>O<sub>2</sub>Pt, 615.580).

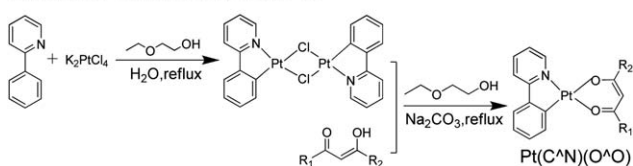
**[Pt(ppy)(NPTPD)] (**3**).** 21% yield. <sup>1</sup>H NMR (400 MHz, CDCl<sub>3</sub>) δ: 9.17 (dd, *J* = 5.78, 5.80 Hz, 1H; pyridine-H), 8.00–8.06 (m, 2H; ArH), 7.78–7.83 (m, 3H; ArH), 7.65 (d, *J* = 7.96 Hz, 1H; ArH), 7.56–7.59 (m, 1H; ArH), 7.48 (d, *J* = 6.61 Hz, 1H; ArH), 7.11–7.18 (m, 4H; ArH), 6.74–6.77 (m, 2H; ArH), 6.71 (s, 1H; ArH), 3.08 (s, 3H; CH<sub>3</sub>), 3.07 (s, 3H; CH<sub>3</sub>); <sup>13</sup>C NMR (100 MHz, CDCl<sub>3</sub>) δ: 40.18, 94.54, 111.30, 118.36, 121.35, 123.05, 123.49, 126.75, 126.86, 127.93, 128.17, 128.86, 128.96, 129.58, 138.04, 146.60, 147.41, 152.31, 168.48, 178.56, 179.25. Anal. calcd for C<sub>26</sub>H<sub>22</sub>N<sub>2</sub>O<sub>2</sub>PtS: C, 50.24; H, 3.57; N, 4.51. Found: C, 50.44; H, 3.83; N, 4.84. MS (ESI) *m/z*: 622.08 ([M]<sup>+</sup>, calcd for C<sub>26</sub>H<sub>22</sub>N<sub>2</sub>O<sub>2</sub>PtS, 622.11).

**[Pt(ppy)(DBM)] (**4**).** 36% yield <sup>1</sup>H NMR (400 MHz, CDCl<sub>3</sub>, 298 K) δ: 9.16 (d, 1H, pyridine-H, *J* = 5.2 Hz), 8.08 (m, 4H, pyridine-H, Ph), 7.83–7.87 (m, 1H, Ph), 7.78 (d, 1H, Ph, *J* = 7.5 Hz), 7.67 (d, 1H, Ph, *J* = 7.8 Hz), 7.55–7.59 (m, 2H, Ph), 7.48–7.52 (m, 5H, Ph), 7.29 (d, 1H, Ph, *J* = 7.2 Hz), 7.12–7.23 (m, 2H, Ph), 6.78 (s, 1H, C–CH=); <sup>13</sup>C NMR (100 MHz, CDCl<sub>3</sub>) δ:

### Synthesis of O<sup>^</sup>O diketonate ligands



### Synthesis of Complexes Pt(C<sup>^</sup>N)(O<sup>^</sup>O)



**Scheme 2** Synthetic routes of the diketonate ligands and complexes [Pt(C<sup>^</sup>N)(O<sup>^</sup>O)].

97.52, 118.52, 121.45, 123.14, 123.78, 127.00, 127.11, 128.62, 128.68, 129.35, 130.80, 130.98, 138.34, 138.93, 139.28, 140.20, 144.83, 147.28, 168.44, 178.90, 179.96. Anal. calcd for  $C_{26}H_{19}NO_2Pt$ : C, 54.55; H, 3.35; N, 2.45. Found: C, 54.13; H, 3.58; N, 2.76. MS (MALDI-TOF/TOF) ( $m/z$ ): 573.291 ( $[M + 1]^+$ , calcd for  $C_{26}H_{19}NO_2Pt$ , 572.106).

**[Pt(ppy)(CPNPD)] (5).** 35% yield.  $^1H$  NMR (400 MHz,  $CDCl_3$ )  $\delta$ : 9.19–9.23 (m, 1H; pyridine-H), 8.65 (d,  $J = 15.64$  Hz, 1H; ArH), 8.33–8.36 (m, 2H; ArH), 8.17–8.23 (m, 3H; ArH), 8.04 (d,  $J = 7.97$  Hz, 1H; ArH), 7.83–7.98 (m, 4H; ArH), 7.68–7.75 (m, 3H; ArH), 7.44–7.63 (m, 6H; ArH), 7.35 (t,  $J = 8.22$  Hz, 2H; ArH), 7.32–7.34 (m, 3H; ArH), 7.16–7.24 (m, 1H; ArH), 7.0 (s, 1H; C–CH=);  $^{13}C$  NMR (100 MHz,  $CDCl_3$ )  $\delta$ : 97.91, 109.88, 118.53, 120.40, 121.41, 123.18, 123.73, 124.23, 126.16, 126.77, 127.28, 127.36, 127.87, 128.33, 128.71, 128.80, 129.15, 130.93, 133.04, 134.55, 134.62, 136.60, 137.55, 137.99, 138.28, 138.97, 139.87, 140.04, 140.43, 144.85, 147.29, 168.51, 178.45, 179.02. Anal. calcd for  $C_{42}H_{28}N_2O_2Pt$ : C, 64.04; H, 3.58; N, 3.56. Found: C, 64.38; H, 3.26; N, 3.33. MS (MALDI-TOF/TOF) ( $m/z$ ): 787.693 ( $[M]^+$ , calcd for  $C_{42}H_{28}N_2O_2Pt$ , 787.762).

### Cell culture

The HeLa cell line was provided by the Institute of Biochemistry and Cell Biology, SIBS, CAS (People's Republic of China). The HeLa cells were grown in MEM (modified Eagle's medium) supplemented with 10% FBS (fetal bovine serum) at 37 °C and 5%  $CO_2$ . Cells ( $5 \times 10^8 L^{-1}$ ) were plated on 14 mm glass cover slips and allowed to adhere for 24 h. The KB cell line was provided by the Institute of Basic Medical Sciences Chinese Academy of Medical Sciences. The KB cells were grown in RPMI 1640 supplemented with 10% FBS at 37 °C and 5%  $CO_2$ .<sup>23</sup>

### Luminescence bioimaging

Prior to experiments, cells were washed with PBS buffer and then incubated solely with 10  $\mu M$  **1** (or **2–5**) in DMSO/PBS (pH = 7; 1/99, v/v) for 30 min at 37 °C. Cell imaging was then carried out after washing the cells with PBS. Confocal luminescence imaging, including xy-scan and Z-scan luminescent imaging, was performed with an Olympus FV1000 laser scanning confocal microscope and a 60  $\times$  oil-immersion objective lens. Excitation of the HeLa cells incubated with **1** (or **2–5**) at 405 nm was carried out with a semiconductor laser. Emission was collected from 480 nm to 580 nm for the HeLa cells incubated solely with **1** (or **2–5**), respectively.

### Cytotoxicity assay

The *in vitro* cytotoxicity was measured using the MTT assay (where MTT is 3-(4,5-dimethylthiazol-2-yl)2,5-diphenyl-tetrazolium bromide).<sup>24</sup> Briefly, cells growing in log phase were seeded into a 96-well cell-culture plate at  $1 \times 10^4$ /well. The cells were incubated for 24 h at 37 °C under 5%  $CO_2$ . The Pt(II) complex (100  $\mu L$ /well) at concentrations of 3, 6.25, 12.5, 25, 50, and 100  $\mu M$  was added to the wells of the treatment group, and 100  $\mu L$ /well DMSO diluted in RPMI 1640 at a final concentration of 0.2% to the negative control group. The cells were incubated for 24 h at 37 °C under 5%  $CO_2$ . The 20  $\mu L$  combined MTT/PBS

solution (5 mg  $mL^{-1}$ ) was added to each well of the 96-well assay plate, and the mixtures were incubated for an additional 3 h. An enzyme-linked immunosorbent assay (ELISA) reader (Bio-Rad, Model 570) was used to measure the OD490 (Absorbance value) of each well referenced at 690 nm. The following formula was used to calculate the viability of cell growth:

$$\text{Viability (\%)} = \frac{(\text{mean of absorbance value of treatment group})}{(\text{mean absorbance value of control})} \times 100$$

The results are expressed as an average over three nominally identical measurements. The statistical significance was tested using one-way analysis of variance followed by the Student-Newman-Keuls test on SPSS 11.0 software. Statistical significance was set at  $P < 0.05$ .

## Results and discussion

### Synthesis of ligands and complexes

Ligands HNDBM, HCPNPD, and HNPTPD were synthesized according to a modified procedure reported in the previous literature.<sup>22</sup> The synthetic procedure for the Pt(II) complexes with the general structure of  $[Pt(C^{\wedge}N)(O^{\wedge}O)]$  includes two steps (Scheme 2). Firstly, the dinuclear cyclometalated Pt(II) chloro-bridged precursor,  $[Pt(ppy)Cl]_2$ , was synthesized according to a literature procedure.<sup>1b,d</sup> Then, by bridge splitting reactions of  $[Pt(ppy)Cl]_2$  and subsequent complexation with  $\beta$ -diketonate ligands, the target Pt(II) complexes can be obtained. All complexes are characterized by  $^1H$  NMR spectroscopy,  $^{13}C$  NMR spectroscopy and MALDI-TOF/TOF MS or ESI MS spectroscopy. Moreover, the structure of complex **4** was further identified by single-crystal X-ray diffraction analysis.

### Crystal structure

The single crystal of **4** was obtained by slow diffusion of hexane into its dichloromethane solution. The ORTEP diagram of **4** is depicted in Fig. 1 and the  $\pi$ – $\pi$  stacking between adjacent ppy ligands of different molecules is shown in Fig. 2. The crystallographic refinement parameters of **4** are summarized in Table S1 (see Electronic Supplementary Information, ESI†). Selected relevant bond parameters are listed in Table S2 (ESI†). All bond lengths and bond angles are characteristic of related

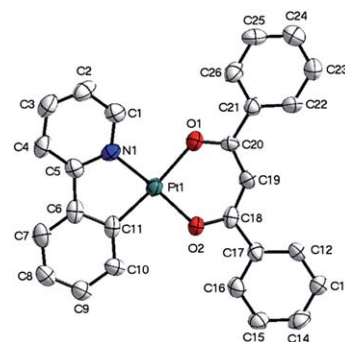


**Fig. 1** ORTEP diagram of **4**. For clarity, the hydrogen atoms are omitted.

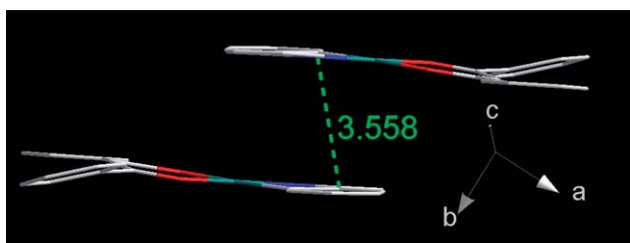


Fig. 2  $\pi$ - $\pi$  interactions between adjacent molecules of **4**.

cyclometalated Pt(II) complexes.<sup>1b,6a</sup> The Pt(1)–C(11) (1.963(7) Å) bond length is similar to the average value reported for the *cis*-(ppy)<sub>2</sub>Pt complex (1.984(4) Å).<sup>25</sup> The Pt(1)–N(1) (1.978(7) Å) bond length is comparable to mean values of 1.984 Å from other Pt(ppy) derivatives.<sup>8a</sup> The Pt(1)–O(1) (2.081(5) Å) and Pt(1)–O(2) (2.014(5) Å) bond lengths are within the range (1.985(6)–2.156(2) Å) of other cyclometalated Pt( $\beta$ -diketonato) derivatives.<sup>1b,c</sup> The C(11)–Pt(1)–N(1) (81.2(3)°) and O(1)–Pt(1)–O(2) (90.71(2)°) bond angles are typical for cyclometalated Pt(II) complexes with  $\beta$ -diketonate ligand (see Table S2†).<sup>1b,c</sup> In addition, the C–Pt–N and O–Pt–O chelate planes are almost coplanar with the dihedral angle of 1.52°.

From Fig. 2 we can see that the Pt(II) complex has a slightly distorted square planar geometry, which is similar to previous structural studies on mononuclear species containing the cyclometalated C<sup>^</sup>N ligands.<sup>8a</sup> The ppy ligands of adjacent molecules pack as head-to-tail dimers and have a plane-to-plane separation of 3.558 Å between adjacent ppy ligands, indicating the presence of strong  $\pi$ - $\pi$  interactions (Fig. 2). In addition, the closest Pt–Pt distance is 4.495 Å, indicating the absence of metal-metal interactions.

### Electrochemical properties

The electrochemical properties of Pt(II) complexes were investigated using cyclic voltammetry (Fig. 3). All of the electrochemical potentials were measured relative to an internal ferrocene reference (Cp<sub>2</sub>Fe/Cp<sub>2</sub>Fe<sup>+</sup>). The HOMO and LUMO energies can be deduced by the equation  $E_{\text{HOMO(LUMO)}} =$

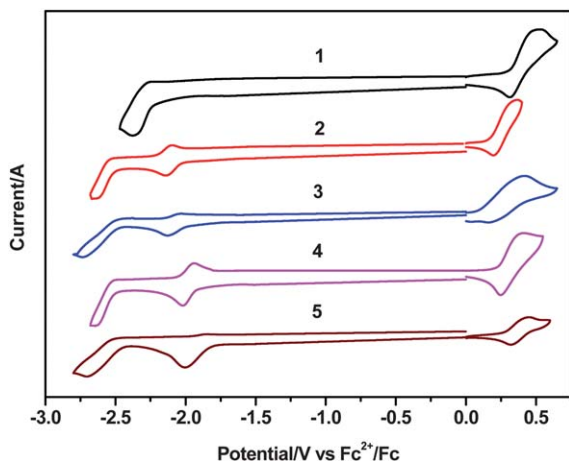


Fig. 3 Cyclic voltammograms of **1–5** (oxidations and reductions were measured in CH<sub>2</sub>Cl<sub>2</sub>, DMF, respectively, scan rate = 50 mV s<sup>-1</sup>).

$-(4.80 + E_{\text{onset}})$ .<sup>26</sup> Also, the energy gap ( $\Delta E$ ) between the HOMO and LUMO can be calculated by the equation  $\Delta E = E_{\text{LUMO}} - E_{\text{HOMO}}$ . The data are summarized in Table 1.

All complexes show a single irreversible oxidation wave between 0.28 and 0.42 V, which is assigned to the oxidation of metal center.<sup>9a,27</sup> According to the DFT calculation, the cyclometalated C<sup>^</sup>N ligand and/or ancillary ligand also contributes to HOMO (Table S3, ESI†). Since square planar Pt(I) and Pt(III) metal centers are susceptible to nucleophilic attack by solvents, the Pt(II) redox processes are usually irreversible.<sup>1b,9a</sup> For complex **1** containing  $\beta$ -diketonate ligand with high triplet-state energy level, only one reduction wave at  $-2.39$  V was observed. Different from **1**, complexes **2–5** were found to have two reduction waves, the first reduction wave ( $-1.93$  to  $-2.12$  V) and the second one ( $-2.60$  to  $-2.73$  V). The first reduction wave can be tentatively assigned to the reduction of O<sup>^</sup>O ligands due to their low triplet energy levels, and the difference of the first reduction potential may be caused by the different electronic structures of the  $\beta$ -diketonate ligands. The second reduction wave is presumably assigned to the reduction of C<sup>^</sup>N ligand.<sup>25,28</sup> This electrochemical behavior is consistent with a description of ligand-localized LUMO distribution and the HOMO with substantial metal character and ligand distribution, as seen in the DFT calculation results. The first reduction potential becomes less negative and the energy gap between the HOMO and LUMO becomes narrower from **1** to **5**, which is in accordance with the red shift of emission wavelength, as discussed below.

### Absorption spectroscopy

The UV-visible absorption spectra of Pt(II) complexes in CH<sub>2</sub>Cl<sub>2</sub> are shown in Fig. 4 and the corresponding electronic absorption data are listed in Table 2. Compared with **1**, complexes **2–5** exhibit more intense absorption bands. Complex **4** has a similar spectral shape to that of **1**. The spectra of **2**, **3**, and **5**, however, are quite different from those of **1** and **4**. All of these complexes display intense absorption bands below 350 nm with extinction coefficients of about 10<sup>5</sup>, which are assigned to spin-allowed  $\pi$ - $\pi^*$  ligand-centered transitions. In addition, complexes **1** and **4** display moderately intense absorption bands in the range 350–450 nm, which are assigned to metal-to-ligand charge transfer (MLCT) and ligand-to-ligand charge transfer (LLCT) transitions. Unusually, very strong absorption bands in the range 350–450 nm are observed for **2**, **3**, and **5**. These bands probably arise from the influence of the strongly electron-donating nature of the amino/carbazole groups in the diketonate ligands.

To clarify the origin of these strong absorption bands in the range 350–450 nm for complexes **2**, **3**, and **5**, and to assign the lowest-lying absorptions of all of the studied complexes, TDDFT calculations have been applied to simulate the absorption properties. The results are discussed in the theoretical calculation section.

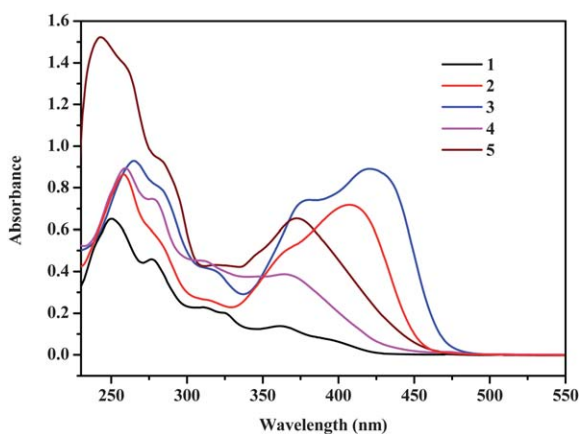
### Luminescence spectroscopy

The room-temperature photoluminescence spectra of Pt(II) complexes in CH<sub>2</sub>Cl<sub>2</sub> solution are shown in Fig. 5 and the corresponding photophysical data are summarized in Table 3. Compared with **1**, the emission wavelengths of complexes **2–5** are

**Table 1** Electrochemical data for complexes 1–5

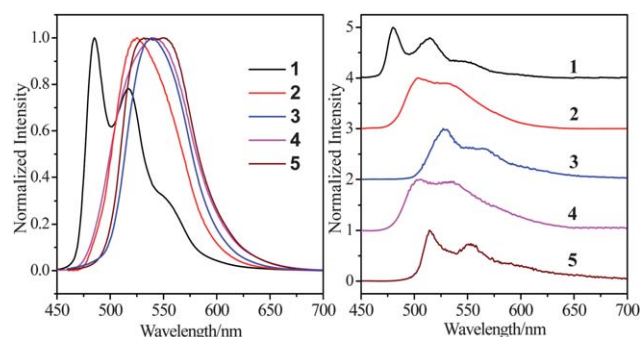
	$E_{\text{onset}}^{\text{ox}}, \text{V}$	$E_{1/2}^{\text{ox}},^a \text{V}$	$E_{1/2}^{\text{re}}$ and $E^{\text{re}},^b \text{V}$	$E_{\text{onset}}^{\text{re}}, \text{V}$	HOMO/LUMO, <sup>c</sup> eV	$\Delta E, \text{eV}$
<b>1</b>	0.36	0.42	−2.39	−2.10	−5.06/−2.40	2.66
<b>2</b>	0.13	0.28	−2.12, −2.60	−2.02	−4.93/−2.78	2.15
<b>3</b>	0.10	0.30	−2.08, −2.73	−1.97	−4.90/−2.83	2.07
<b>4</b>	0.16	0.33	−1.95, −2.60	−1.91	−4.95/−2.89	2.06
<b>5</b>	0.21	0.39	−1.93, −2.70	−1.82	−5.01/−2.98	2.03

<sup>a</sup> In  $\text{CH}_2\text{Cl}_2$  (0.10 mol  $\text{L}^{-1}$  of  $\text{Bu}_4\text{NPF}_6$ ) at 298 K, scan rate of 50  $\text{mV s}^{-1}$ . <sup>b</sup> In DMF (0.10 mol  $\text{L}^{-1}$  of  $\text{Bu}_4\text{NPF}_6$ ) at 298 K, scan rate of 50  $\text{mV s}^{-1}$ . <sup>c</sup> Values calculated using  $-4.8 \text{ eV}$  for ferrocene.

**Fig. 4** Absorption spectra of 1–5 at room temperature in  $\text{CH}_2\text{Cl}_2$  solution.

red-shifted significantly. By changing the  $\beta$ -diketonate ligands of complexes 1–5, their emission wavelengths were tuned from 485 to 550 nm. This is consistent with the decrease of  $\Delta E$  deduced from electrochemical data. Considering that all of the Pt(II) complexes have the same C<sup>N</sup> ligand, we can deduce that the decrease of  $\Delta E$  and the red-shift of the emission wavelength must be due to the variation in the  $\beta$ -diketonate ligand. The effect of conjugation length on the energy levels of the  $\beta$ -diketonate ligands can be seen by the variation in their singlet energy levels, which relate to the wavelengths of their UV-visible absorbance edges (see Fig. S1, ESI<sup>†</sup>). The wavelengths of the UV-visible absorption edges of acac, NDBM, NPTPD, DBM, and CPNPD are 304, 449, 361, 384, and 436 nm, respectively, indicating that their corresponding singlet energy levels are 32895, 22272, 21692, 26042, and 22936  $\text{cm}^{-1}$ , respectively (see Table S4, ESI<sup>†</sup>).

Fig. 5 shows that the photoluminescence spectrum of 1 displays a vibronic progression, while those of 2–5 are broad and structureless at room temperature, indicating that the excited-state properties of 2–5 are different from those of 1. Interestingly,

**Fig. 5** Photoluminescence spectra of 1–5 in  $\text{CH}_2\text{Cl}_2$  solution ( $\lambda_{\text{ex}} = 365 \text{ nm}$ ) at room temperature (left) and 77 K (right).

complex 5 exhibits two emissive peaks at 532 and 550 nm, which originate from the same excited state according to their similar excitation spectra, which are provided in the ESI (see Fig. S2<sup>†</sup>).

The photoluminescence spectra of all of the Pt(II) complexes in different solvents have been studied to investigate their excited-state properties, and the data are summarized in Table 3. No obvious shifts in the photoluminescence spectra of the respective complexes were observed upon changing the solvent. Furthermore, the low-temperature (77 K) photoluminescence spectra (Fig. 5) of all of the complexes were also recorded. For 1, no evident blue-shift of the emission maximum was observed on going from fluid solution at room temperature to rigid matrix at 77 K (Table 3). For complexes 2–5, however, obvious blue-shifts of the emission maxima were observed, further indicating that the excited-state properties of 2–5 are different from those of 1.

According to previous work,<sup>29</sup> photoluminescence spectra from the ligand-centered  ${}^3\pi-\pi^*$  state display vibronic progressions, while those from the charge-transfer (CT) state are broad and featureless. Therefore, we can conclude that the charge-transfer state participates in the excited states for 2–5. The sensitivity of the photoluminescence spectra of 2–5 to temperature further shows that the excited states of these complexes can

**Table 2** Absorption data of 1–5 in  $\text{CH}_2\text{Cl}_2$  at  $2.0 \times 10^{-5} \text{ mol L}^{-1}$ 

Complex	$\lambda_{\text{abs}}(\log \epsilon)$ [nm]
<b>1</b>	250(4.49), 276(4.34), 311(4.01), 326(3.95,sh), 361(3.76), 400(3.30,sh)
<b>2</b>	258(4.64), 282(4.44,sh), 316(4.11,sh), 363(4.39,sh), 408(4.56)
<b>3</b>	260(4.67), 280(4.59,sh), 314(4.30,sh), 332(4.16), 376(4.57), 415(4.65)
<b>4</b>	259(4.65), 277(4.57), 311(4.35), 348(4.27,sh), 363(4.29)
<b>5</b>	238(4.88), 256(4.83,sh), 280(4.66,sh), 313(4.33), 329(4.32), 367(4.51)

**Table 3** Emission data of **1–5** in different conditions

	$\lambda_{\text{PL, max}}^a$ (nm)						$\Phi_{\text{em}}^b$
	CH <sub>2</sub> Cl <sub>2</sub>	CH <sub>3</sub> CN	THF	DMSO/PBS <sup>c</sup> (1 : 99, v/v)	Solid film	Glass (77 K)	
<b>1</b>	485, 515(sh)	483	486	493,528	528	480	0.11
<b>2</b>	525	519	515	522	538	503	0.044
<b>3</b>	539	520	528	532	552	527	0.018
<b>4</b>	541	543	537	545	557	506	0.086
<b>5</b>	550, 532(sh)	552	550	543,560	562	514	0.11

<sup>a</sup> Room temperature,  $\lambda_{\text{ex}} = 365$  nm. <sup>b</sup> The solvent is CH<sub>2</sub>Cl<sub>2</sub> and *fac*-Ir(ppy)<sub>3</sub> was used as a reference. <sup>c</sup> PBS: phosphate buffer solution.

be mainly attributed to the CT states (including the <sup>3</sup>MLCT and <sup>3</sup>LLCT) and that the contribution from <sup>3</sup>LC ( $\pi_{\text{C}^{\wedge}\text{N}}\pi^*_{\text{C}^{\wedge}\text{N}}$ ) is relatively small.<sup>30</sup> Furthermore, the photoluminescence spectra of **2**, **4**, and **5** exhibit small dependencies on the solvent polarity. It can thus be concluded that the emissions of **2–5** are caused by the particular CT states mixed with a little ligand-centered (C<sup>^</sup>N) character (<sup>3</sup>LC), while the emission of **1** is mainly caused by ligand-centered (C<sup>^</sup>N) character (<sup>3</sup>LC) due to the vibronic progression of the photoluminescence spectrum and its small dependence on the solvent polarity and temperature.<sup>31</sup> Hence, by modifying the chemical structures of the  $\beta$ -diketonate ligands, the excited states of cyclometalated Pt(II) complexes can be tuned.

It is worth noting that the emission color of the five Pt(II) complexes considered here can be tuned from blue-green to yellow by simply changing the  $\beta$ -diketonate ligands (Fig. 6). Thus, this work provides a simple means of tuning the emission properties of Pt(II) complexes. The present complexes show moderately intense emissions with different luminescence quantum yields. The luminescence quantum yield of complex **1** is 11%, while complexes **2–5** have quantum yields of 1.8–11%. Complex **5** has a quantum yield comparable to that of **1**. In view of the fact that complexes **1–5** have the same cyclometalated ligand (ppy), we can deduce that the different luminescence quantum yields in solution must be due to the variation in the electronic structures of the  $\beta$ -diketonate ligands.

To rationalize the significant variation in emission properties, the triplet energy levels of the three ancillary ligands Hacac, HNDBM, and HDBM (Scheme 1) were estimated by referring to the lower-wavelength emission edges of their corresponding phosphorescence spectra. The relevant data are provided in Table S4 (ESI<sup>†</sup>). The triplet energy levels of the ancillary ligands (<sup>3</sup>LX) conform to the following sequence: <sup>3</sup>LX<sub>acac</sub> > <sup>3</sup>LX<sub>DDBM</sub> > <sup>3</sup>LX<sub>NDBM</sub>. For complex **1**, the triplet state of the ligand ppy and



**Fig. 6** Luminescence photographs of **1–5** in CH<sub>2</sub>Cl<sub>2</sub> solution ( $\lambda_{\text{ex}} = 365$  nm).

the MLCT excited state lie lower in energy than those of the ancillary ligand acac.<sup>11a</sup> Thus, its luminescence is dominated by <sup>3</sup>LC<sub>ppy</sub> and <sup>3</sup>ML<sub>ppy</sub>CT transitions. For **2–5**, the low triplet energy of the ancillary ligand rather than that of ppy dominates the excited state, and the contribution from ppy is relatively small, as further discussed in the following text.

### Theoretical calculations on excited state properties of **1–5**

To further understand the photophysical properties of complexes **1–5**, a theoretical analysis based on DFT/TDDFT approach was provided. The calculated absorption spectra of **1–5** in CH<sub>2</sub>Cl<sub>2</sub> solution are shown in Fig. S3 (ESI<sup>†</sup>) and the selective calculated results (the states with high oscillator strength) for the lowest-lying transitions are summarized in Table S5 (ESI<sup>†</sup>). The distribution of important frontier orbitals (HOMOs and LUMOs) at the ground state are shown in the ESI (Table S3<sup>†</sup>).

It can be seen from Fig. S3 (ESI<sup>†</sup>) that the calculated lowest-lying absorptions of **1–5** are very similar to those measured experimentally. The lowest-lying singlet state of **1** mainly originates from the HOMO → LUMO transition, which can be described as <sup>1</sup>LC (<sup>1</sup> $\pi_{\text{C}^{\wedge}\text{N}}\pi^*_{\text{C}^{\wedge}\text{N}}$ ) mixed with <sup>1</sup>MLCT (<sup>1</sup> $d\pi^*_{\text{C}^{\wedge}\text{N}}$ ) (Table S5, ESI<sup>†</sup>). That of **4** mainly originates from the HOMO → LUMO + 1 transition, which can be assigned as a mixture of <sup>1</sup>MLCT (<sup>1</sup> $d\pi^*_{\text{O}^{\wedge}\text{O}}$ ), <sup>1</sup>MLCT (<sup>1</sup> $d\pi^*_{\text{C}^{\wedge}\text{N}}$ ), <sup>1</sup>LLCT ( $\pi_{\text{C}^{\wedge}\text{N}}\pi^*_{\text{O}^{\wedge}\text{O}}$ ), and <sup>1</sup>LC ( $\pi_{\text{C}^{\wedge}\text{N}}\pi^*_{\text{C}^{\wedge}\text{N}}$ ). Those of **2**, **3**, and **5** mainly originate from HOMO → LUMO transitions, which comprise <sup>1</sup>ILCT (<sup>1</sup> $\pi_{\text{O}^{\wedge}\text{O}}\pi^*_{\text{O}^{\wedge}\text{O}}$ ) and <sup>1</sup>MLCT (<sup>1</sup> $d\pi^*_{\text{O}^{\wedge}\text{O}}$ ) transitions. Hence, the intense absorption bands of **2**, **3**, and **5** in the range 350–450 nm can be assigned to mixtures of <sup>1</sup>ILCT (<sup>1</sup> $\pi_{\text{O}^{\wedge}\text{O}}\pi^*_{\text{O}^{\wedge}\text{O}}$ ) and <sup>1</sup>MLCT transitions. The HOMOs of **2**, **3**, and **5** primarily reside on the  $\pi$  electron donors (D) of the  $\beta$ -diketonate ligands, while their LUMOs are predominantly located on the  $\pi$  electron acceptors (A) of these ligands (Table S3, ESI<sup>†</sup>). Thus, the strong absorption bands in the 350–450 nm region may be caused by the strongly electron-donating nature of the amino or carbazole groups of the  $\beta$ -diketonate ligands. Phosphorescent dyes with strong absorption bands in the visible range are of great importance. Hence, the combination of D- $\pi$ -A structures in  $\beta$ -diketonate ligands with the rich photochemical and photophysical properties of Pt(II) complexes may lead to some new properties for research. In addition, it was found that the respective ligands show some differences between **1** and **2–5**, that is, the singlet excited states of **1** related to absorption are dominated by the C<sup>^</sup>N ligand, while those of **2–5** are mainly dominated by the diketonate ligands and the contribution from the

C<sup>N</sup> ligand is relatively small. This is in accordance with the experimental results.

We also investigated the emission properties of the complexes on the basis of the calculated results. The excited states responsible for the emission of complexes 1–5 were obtained through the calculation at the triplet optimized geometry by TDDFT in CH<sub>2</sub>Cl<sub>2</sub> solution and the selective calculated results are listed in Table 4. The distribution of important frontier orbitals (HOMOs and LUMOs) at the triplet state are shown in Fig. 7.

For complex 1, the T<sub>1</sub> excited state, which is responsible for the emission, is derived from two transitions (Table 4): H → L (0.69) (H and L refer to the HOMO and LUMO respectively) and H-1 → L (0.27). Both of them can be described as mixtures of <sup>3</sup>LC (<sup>3</sup>π<sub>C<sup>N</sup></sub>π\*<sub>C<sup>N</sup></sub>), <sup>3</sup>MLCT (<sup>3</sup>dπ\*<sub>C<sup>N</sup></sub>), and <sup>3</sup>LLCT (<sup>3</sup>π<sub>O<sup>Λ</sup>O</sub>π\*<sub>C<sup>N</sup></sub>). Hence, the luminescence of 1 is dominated by <sup>3</sup>LC and <sup>3</sup>MLCT transitions of the ligand ppy, which is consistent with the experimental results mentioned above.

The T<sub>1</sub> excited state of complex 2 is derived from two transitions: H → L (0.63) and H-1 → L (0.34), which can be described as a mixture of <sup>3</sup>ILCT (<sup>3</sup>π<sub>O<sup>Λ</sup>O</sub>π\*<sub>O<sup>Λ</sup>O</sub>), <sup>3</sup>MLCT (<sup>3</sup>dπ\*<sub>O<sup>Λ</sup>O</sub>), and <sup>3</sup>LLCT (<sup>3</sup>π<sub>C<sup>N</sup></sub>π\*<sub>O<sup>Λ</sup>O</sub>). Complex 3 has a T<sub>1</sub> state derived from H → L (0.59) and H-1 → L (0.37), which can be described as <sup>3</sup>LLCT (<sup>3</sup>π<sub>C<sup>N</sup></sub>π\*<sub>O<sup>Λ</sup>O</sub>)/<sup>3</sup>ILCT (<sup>3</sup>π<sub>O<sup>Λ</sup>O</sub>π\*<sub>O<sup>Λ</sup>O</sub>)/<sup>3</sup>MLCT (<sup>3</sup>dπ\*<sub>O<sup>Λ</sup>O</sub>). For complex 4, the T<sub>1</sub> state is composed mainly of two excitation configurations: H → L (0.61) described as <sup>3</sup>LLCT (<sup>3</sup>π<sub>C<sup>N</sup></sub>π\*<sub>O<sup>Λ</sup>O</sub>)/<sup>3</sup>MLCT (<sup>3</sup>dπ\*<sub>O<sup>Λ</sup>O</sub>) and H-1 → L (0.43) described

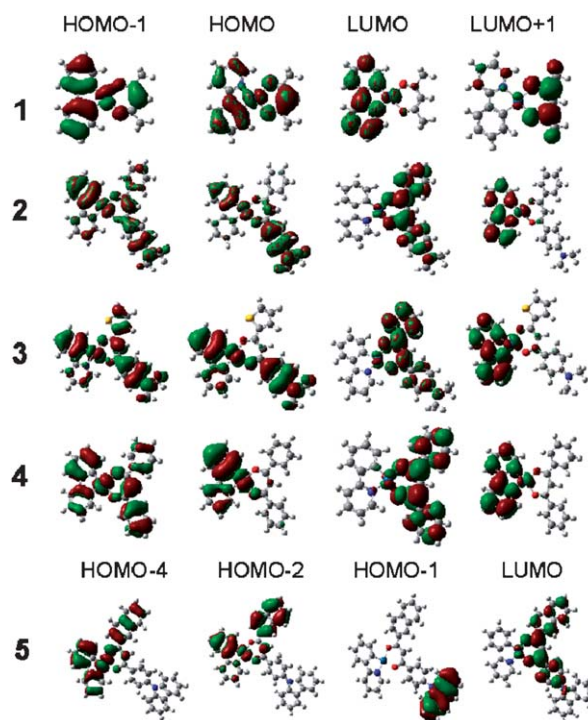


Fig. 7 HOMOs and LUMOs distributions of 1–5 at the triplet states.

**Table 4** Electronic transitions of 1–5 calculated at the triplet optimized geometry by TDDFT in CH<sub>2</sub>Cl<sub>2</sub> solution. The solvent effect is modeled by the PCM method

Complex	State	Wavelength (nm)	<i>f</i>	Assignment	Description
1	T <sub>1</sub>	575.3	0	H → L (0.69)	<sup>3</sup> MLCT ( <sup>3</sup> dπ* <sub>C<sup>N</sup></sub> )/ <sup>3</sup> LLCT ( <sup>3</sup> π <sub>O<sup>Λ</sup>O</sub> π* <sub>C<sup>N</sup></sub> )/ <sup>3</sup> LC ( <sup>3</sup> π <sub>C<sup>N</sup></sub> π* <sub>C<sup>N</sup></sub> )
				H-1 → L (0.27)	<sup>3</sup> MLCT ( <sup>3</sup> dπ* <sub>C<sup>N</sup></sub> )/ <sup>3</sup> LLCT ( <sup>3</sup> π <sub>O<sup>Λ</sup>O</sub> π* <sub>C<sup>N</sup></sub> )/ <sup>3</sup> LC ( <sup>3</sup> π <sub>C<sup>N</sup></sub> π* <sub>C<sup>N</sup></sub> )
2	T <sub>1</sub>	592.6	0	H → L (0.63)	<sup>3</sup> ILCT ( <sup>3</sup> π <sub>O<sup>Λ</sup>O</sub> π* <sub>O<sup>Λ</sup>O</sub> )/ <sup>3</sup> MLCT ( <sup>3</sup> dπ* <sub>O<sup>Λ</sup>O</sub> )/ <sup>3</sup> LLCT ( <sup>3</sup> π <sub>C<sup>N</sup></sub> π* <sub>O<sup>Λ</sup>O</sub> )
				H-1 → L (0.34)	<sup>3</sup> ILCT ( <sup>3</sup> π <sub>O<sup>Λ</sup>O</sub> π* <sub>O<sup>Λ</sup>O</sub> )/ <sup>3</sup> MLCT ( <sup>3</sup> dπ* <sub>O<sup>Λ</sup>O</sub> )/ <sup>3</sup> LLCT ( <sup>3</sup> π <sub>C<sup>N</sup></sub> π* <sub>O<sup>Λ</sup>O</sub> )
				H-1 → L (0.55)	<sup>3</sup> ILCT ( <sup>3</sup> π <sub>O<sup>Λ</sup>O</sub> π* <sub>O<sup>Λ</sup>O</sub> )/ <sup>3</sup> MLCT ( <sup>3</sup> dπ* <sub>O<sup>Λ</sup>O</sub> )/ <sup>3</sup> LLCT ( <sup>3</sup> π <sub>C<sup>N</sup></sub> π* <sub>O<sup>Λ</sup>O</sub> )
3	T <sub>1</sub>	640.8	0	H → L (0.59)	<sup>3</sup> LLCT ( <sup>3</sup> π <sub>C<sup>N</sup></sub> π* <sub>O<sup>Λ</sup>O</sub> )/ <sup>3</sup> ILCT ( <sup>3</sup> π <sub>O<sup>Λ</sup>O</sub> π* <sub>O<sup>Λ</sup>O</sub> )/ <sup>3</sup> MLCT ( <sup>3</sup> dπ* <sub>O<sup>Λ</sup>O</sub> )
				H-1 → L (0.37)	<sup>3</sup> LLCT ( <sup>3</sup> π <sub>C<sup>N</sup></sub> π* <sub>O<sup>Λ</sup>O</sub> )/ <sup>3</sup> ILCT ( <sup>3</sup> π <sub>O<sup>Λ</sup>O</sub> π* <sub>O<sup>Λ</sup>O</sub> )/ <sup>3</sup> MLCT ( <sup>3</sup> dπ* <sub>O<sup>Λ</sup>O</sub> )
				H → L (0.48)	<sup>3</sup> LLCT ( <sup>3</sup> π <sub>C<sup>N</sup></sub> π* <sub>O<sup>Λ</sup>O</sub> )/ <sup>3</sup> ILCT ( <sup>3</sup> π <sub>O<sup>Λ</sup>O</sub> π* <sub>O<sup>Λ</sup>O</sub> )/ <sup>3</sup> MLCT ( <sup>3</sup> dπ* <sub>O<sup>Λ</sup>O</sub> )
4	T <sub>1</sub>	597.6	0	H → L (0.61)	<sup>3</sup> LLCT ( <sup>3</sup> π <sub>C<sup>N</sup></sub> π* <sub>O<sup>Λ</sup>O</sub> )/ <sup>3</sup> MLCT ( <sup>3</sup> dπ* <sub>O<sup>Λ</sup>O</sub> )
				H-1 → L (0.43)	<sup>3</sup> LLCT ( <sup>3</sup> π <sub>C<sup>N</sup></sub> π* <sub>O<sup>Λ</sup>O</sub> )/ <sup>3</sup> MLCT ( <sup>3</sup> dπ* <sub>O<sup>Λ</sup>O</sub> )
				H-1 → L (0.56)	<sup>3</sup> LLCT ( <sup>3</sup> π <sub>C<sup>N</sup></sub> π* <sub>O<sup>Λ</sup>O</sub> )/ <sup>3</sup> MLCT ( <sup>3</sup> dπ* <sub>O<sup>Λ</sup>O</sub> )
5	T <sub>1</sub>	612.7	0	H → L (0.36)	<sup>3</sup> LLCT ( <sup>3</sup> π <sub>C<sup>N</sup></sub> π* <sub>O<sup>Λ</sup>O</sub> )/ <sup>3</sup> MLCT ( <sup>3</sup> dπ* <sub>O<sup>Λ</sup>O</sub> )
				H-1 → L (0.52)	<sup>3</sup> LLCT ( <sup>3</sup> π <sub>C<sup>N</sup></sub> π* <sub>O<sup>Λ</sup>O</sub> )/ <sup>3</sup> MLCT ( <sup>3</sup> dπ* <sub>O<sup>Λ</sup>O</sub> )
				H-2 → L (0.33)	<sup>3</sup> LLCT ( <sup>3</sup> π <sub>C<sup>N</sup></sub> π* <sub>O<sup>Λ</sup>O</sub> )/ <sup>3</sup> MLCT ( <sup>3</sup> dπ* <sub>O<sup>Λ</sup>O</sub> )
5	T <sub>2</sub>	506.5	0	H → L (0.36)	<sup>3</sup> LLCT ( <sup>3</sup> π <sub>C<sup>N</sup></sub> π* <sub>O<sup>Λ</sup>O</sub> )/ <sup>3</sup> MLCT ( <sup>3</sup> dπ* <sub>O<sup>Λ</sup>O</sub> )
				H-4 → L (0.57)	<sup>3</sup> LLCT ( <sup>3</sup> π <sub>C<sup>N</sup></sub> π* <sub>O<sup>Λ</sup>O</sub> )/ <sup>3</sup> MLCT ( <sup>3</sup> dπ* <sub>O<sup>Λ</sup>O</sub> )

as  ${}^3\text{LC} ({}^3\pi_{\text{O}^{\wedge}\text{O}}\pi^*_{\text{O}^{\wedge}\text{O}})/{}^3\text{LLCT} ({}^3\pi_{\text{C}^{\wedge}\text{N}}\pi^*_{\text{O}^{\wedge}\text{O}})/{}^3\text{MLCT} ({}^3\text{d}\pi^*_{\text{O}^{\wedge}\text{O}})$ . The  $T_1$  state of complex **5** consists of H-1  $\rightarrow$  L (0.52) and H-2  $\rightarrow$  L (0.33), described as  ${}^3\text{ILCT} ({}^3\pi_{\text{O}^{\wedge}\text{O}}\pi^*_{\text{O}^{\wedge}\text{O}})/{}^3\text{LMCT} ({}^3\pi_{\text{O}^{\wedge}\text{O}}\text{d})$  and  ${}^3\text{LC} ({}^3\pi_{\text{O}^{\wedge}\text{O}}\pi^*_{\text{O}^{\wedge}\text{O}})/{}^3\text{LLCT} ({}^3\pi_{\text{C}^{\wedge}\text{N}}\pi^*_{\text{O}^{\wedge}\text{O}})/{}^3\text{MLCT} ({}^3\text{d}\pi^*_{\text{O}^{\wedge}\text{O}})$ , respectively.

Evidently, the introduction of the ancillary diketonate ligands significantly changed the excited-state properties of **2–5** compared to those of **1**. It is the diketonate ligands rather than the ligand ppy, that dominate the excited states of complexes **2–5**, which is consistent with the experimental results.

### Emission phenomena in the solid state

The room-temperature photoluminescence spectra of all Pt(II) complexes in solid film are shown in Fig. 8, and the corresponding photoluminescence data of complexes are summarized in Table 3. Complexes **1–5** show yellow emissions with wavelengths from 528 to 562 nm in the solid state at room temperature. In addition, the photoluminescence spectra of these complexes in the solid state are red-shifted compared to those in  $\text{CH}_2\text{Cl}_2$  solution, which can be attributed to the formation of aggregated states.

To better understand the origin of the solid-state emission properties of these Pt(II) complexes, DFT calculations on **4** (as an example) in the solid state were carried out. By referring to the X-ray diffraction data, we calculated the frontier orbital of **4** in the solid state. The optimized structures were found to be very consistent with the X-ray data. On the basis of calculation results, we have found that when the distance between adjacent ppy ligands of different molecules was shortened to 3.6 Å, the LUMO in the solid state delocalized over the DBM ligand, while the HOMO delocalized over both the metal center and the ppy ligands (Fig. 9). Thus, this state mimics the solid-state situation: the crystal packing of **4** exhibits a strong  $\pi$ – $\pi$  interaction between adjacent ppy ligands, with a face-to-face separation of 3.56 Å. It has been well established that in square-planar Pt(II) complexes Pt–Pt interactions and/or  $\pi$ – $\pi$  stacking of the ligands may induce the appearance of emission in the solid state.<sup>32</sup> It is clear that, due to strong  $\pi$ – $\pi$  interactions, the ppy ligands participate significantly in the excited states of **4** in the solid state.

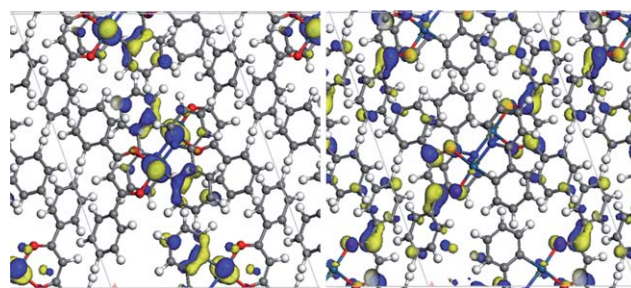


Fig. 9 Calculated HOMO (left) and LUMO (right) distributions of **4** in aggregation state.

Thus, the solid-state emission can be ascribed to a mixture of triplet ligand-ligand-to-ligand charge transfer [ $\pi_{\text{C}^{\wedge}\text{N}}-\pi_{\text{C}^{\wedge}\text{N}} \rightarrow \pi^*_{\text{O}^{\wedge}\text{O}}$ ] ( ${}^3\text{LL}'\text{CT}$ ) and triplet metal-to-ligand charge transfer [ $\text{d}\pi(\text{Pt}) \rightarrow \pi^*_{\text{DBM}}$ ] ( ${}^3\text{MLCT}$ ) transitions.

### Cytotoxicity measurements

The application of phosphorescent heavy-metal complexes in bioimaging is a promising and active research field. Hence, the cytotoxicity or cell viability of **1–5** was assessed to demonstrate their potential utility for bioimaging. Viability assays in a KB cell line were conducted *via* the MTT assay at 24 h.<sup>24</sup> In the presence of the Pt(II) complex with concentration of 3–100  $\mu\text{M}$ , the cellular viabilities were estimated to detect the cytotoxicity (Table 5). The viability data for KB cells after treatment with several concentrations of **1–5** for 24 h are shown in Table 5 and Fig. S4–S8 (see ESI†). The data indicate that all complexes can be considered to be of low cytotoxicity under the experimental conditions used for luminescence cell imaging. It can be seen from Table 5, both **1** and **5** has low cytotoxicity (>80% viability) over a concentration range from 3 to 12.5  $\mu\text{M}$ , appropriate for cell imaging. For **2**, the cellular viabilities were estimated to be larger than 85% with the complex concentration of 25  $\mu\text{M}$ , indicating a lower cytotoxicity for luminescent cell imaging than that of **1** and **5**. Fig. S7 shows that **4** has low cytotoxicity ( $\approx$  85% viability) over a concentration range from 3 to 100  $\mu\text{M}$ , also appropriate for cell imaging. It is worth noting that the cell viability was as high as  $\approx$  90% after addition of 100  $\mu\text{M}$  complex **3**, indicating the lowest cytotoxicity among these complexes. These data show that all complexes exhibit low cytotoxicity for luminescent bioimaging at the concentration of <12.5  $\mu\text{M}$ .

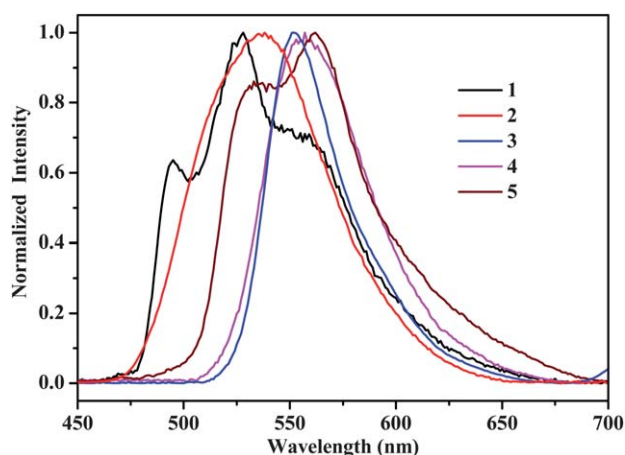


Fig. 8 Emission of **1–5** at room temperature in solid film ( $\lambda_{\text{ex}} = 365$  nm).

Table 5 Cytotoxicity of complexes **1–5**

		Viability (%) under different concentrations of <b>1–5</b> <sup>a</sup>						
Cell		0	3	6.25	12.5	25	50	100
<b>1</b>	KB	100	91.88	87.17	82.34	75.63	75.03	72.51
<b>2</b>	KB	100	99.87	91.58	92.24	85.18	78.18	73.79
<b>3</b>	KB	100	99.7	99.35	99.25	99.11	94.87	88.84
<b>4</b>	KB	100	95.23	92.74	91.3	91.84	88.17	84.82
<b>5</b>	KB	100	97.92	90.22	87.34	79.66	73.73	62.18

<sup>a</sup> KB is cultured in the presence of 3–100  $\mu\text{M}$  **1** (or **2–5**) at 37 °C for 24 h.

## Live cell imaging

Practical application of **1–5** in luminescent imaging of HeLa live cells was investigated using a confocal luminescence microscopy. Due to the poor water solubility of these complexes, the mixed solvent of DMSO/PBS (pH 7; 1/99, v/v) was chosen for bio-imaging experiments. The untreated HeLa cells showed negligible background fluorescence. After sole incubation of cells with 10  $\mu$ M solutions of **1–5** in DMSO/PBS (pH 7; 1/99, v/v) for 30 min at 37  $^{\circ}$ C, strong intracellular luminescences with **1–4** were observed. Differential interference contrast (DIC) bright-field measurements after treatment with **1–4** confirmed that the cells remained viable throughout the imaging experiments. The overlay of confocal luminescence and DIC images showed that the luminescence was evident in the cytoplasm, but not in the nucleus and membrane (Fig. 10). These observations suggest that the complexes were internalized into the cells rather than merely staining the membrane surface. However, only very weak intracellular luminescence was observed for **5** (Fig. 10). This may have been due to weak cellular uptake of **5** owing to its strongly hydrophobic carbazole and naphthalene groups. In addition, the poor solubility of **5** in the DMSO/PBS mixture may also be a reason for its weak cellular uptake. To the best of our knowledge, this is the first example of the application of neutral Pt(II) complexes containing  $\beta$ -diketonate ligands as phosphorescent dyes for live cell imaging.

## Conclusions

In summary, we have demonstrated that a series of Pt(II) complexes based on different  $\beta$ -diketonate ligands with low triplet-state energy levels can exhibit intense photoluminescence

emission in solution. Detailed studies of their electrochemical and photophysical properties have shown that the excited states of these complexes are complicated and can be attributed to mixtures of  $^3\text{MLCT}$ ,  $^3\text{LLCT}$ , and  $^3\text{LC}^{\beta}\text{ILCT}$  transitions. Importantly, significant emission color tuning (from blue-green to yellow) has been achieved by simply changing the  $\beta$ -diketonate ligands. Moreover, by analyzing the influence of molecular packing on the photophysical properties with the help of DFT calculations, it has been found that the solid-state emission may be rationalized in terms of a mechanism of  $^3\text{LLL}^{\beta}\text{CT}$ -mediated phosphorescent emission mixed with  $^3\text{MLCT}$  transition. That is to say, the formation of excimers by  $\pi$ - $\pi$  stacking of adjacent ppy ligands can significantly alter the excited-state properties of the Pt(II) complexes. Furthermore, these complexes have been successfully applied in the luminescence imaging of living cells. Pt(II) complexes **1–4** exhibit low cytotoxicity, good cell membrane permeability, and exclusive staining of the cytoplasm of live cells. All of these features make them promising candidates for the design of specific bioimaging agents. Considering the rich choice of both C $^{\wedge}$ N and O $^{\wedge}$ O ligands and their easy functionalization, it can be envisaged that cyclometalated Pt(II) complexes containing  $\beta$ -diketonate ligands might be developed as an important class of phosphorescent bioimaging dyes. Studies aimed at further functionalization and improvement of the water solubilities of this series of Pt(II) complexes are underway in our laboratories.

## Acknowledgements

This work was financially supported by the National Basic Research Program of China (973 Program, 2009CB930601), National Natural Science Foundation of China (20701009, 50803028, 20804019 and 60976019), Natural Science Foundation

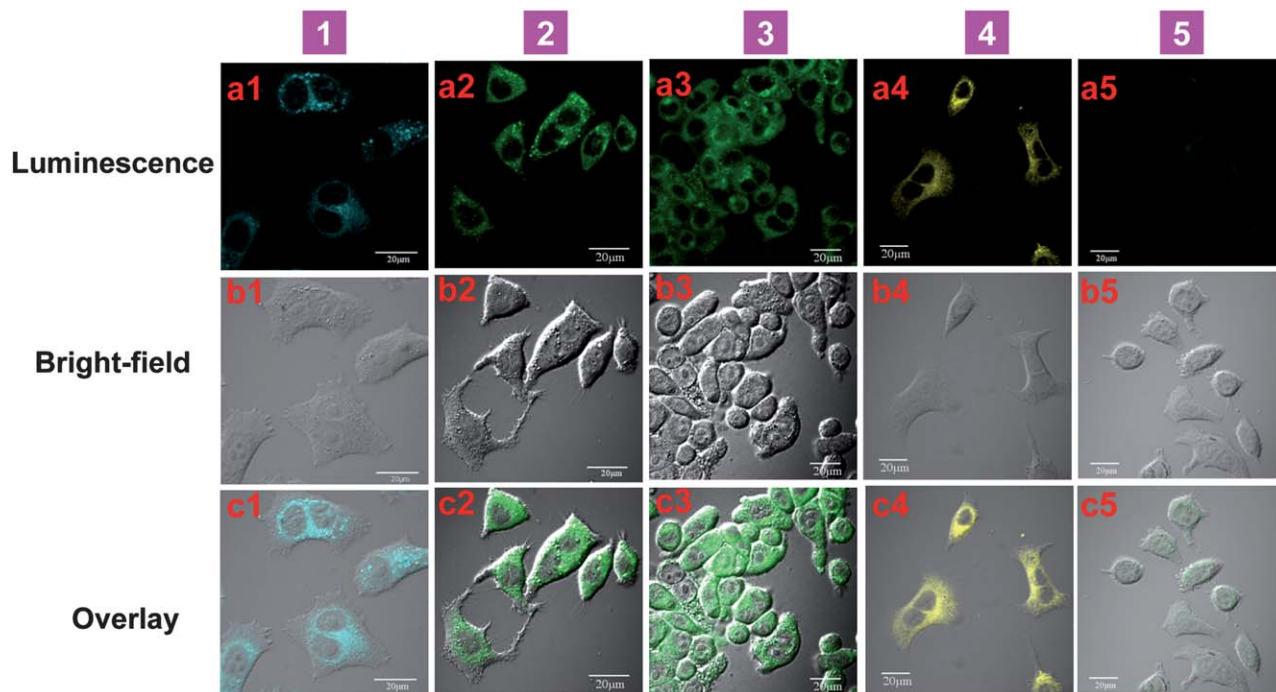


**Fig. 10** Confocal luminescence (a), bright-field (b) and overlay (c) images of HeLa cells incubated solely with 10  $\mu$ M **1–5** in DMSO/PBS (pH 7; 1 : 99, v/v) for 30 min at 37  $^{\circ}$ C. The excitation wavelength is 405 nm.

of Jiangsu Province of China (BK2009427), Natural Science Fund for Colleges and Universities in Jiangsu Province (10KJB430010) and Program for Postgraduates Research Innovation of Colleges and Universities in Jiangsu Province (CX09S\_011Z).

## Notes and references

- (a) Z. He, W. Y. Wong, X. M. Yu, H. S. Kwok and Z. Y. Lin, *Inorg. Chem.*, 2006, **45**, 10922; (b) J. Brooks, Y. Babayan, S. Lamansky, P. I. Djurovich, I. Tsyba, R. Bau and M. E. Thompson, *Inorg. Chem.*, 2002, **41**, 3055; (c) B. Ma, P. I. Djurovich, M. Yousuffuddin, R. Bau and M. E. Thompson, *J. Phys. Chem. C*, 2008, **112**, 8022; (d) D. N. Kozhevnikov, V. N. Kozhevnikov, M. M. Ustinova, A. Santoro, D. W. Bruce, B. Koenig, R. Czerwieniec, T. Fischer, M. Zabel and H. Yersin, *Inorg. Chem.*, 2009, **48**, 4179; (e) Y. Chi and P. T. Chou, *Chem. Soc. Rev.*, 2010, **39**, 638; (f) Q. Zhao, S. J. Liu and W. Huang, *Macromol. Rapid Commun.*, 2010, **31**, 794; (g) W. Y. Wong and C. L. Ho, *Coorg. Chem. Rev.*, 2009, **253**, 1709; (h) W. Y. Wong and C. L. Ho, *J. Mater. Chem.*, 2009, **19**, 4457; (i) W. Y. Wong, Z. He, S. K. So, K. L. Tong and Z. Y. Lin, *Organometallics*, 2005, **24**, 4079.
- (a) A. Y. Y. Tam, K. M. C. Wong and V. W. W. Yam, *J. Am. Chem. Soc.*, 2009, **131**, 6253; (b) S. Y. Chang, J. L. Chen, Y. Chi, Y. M. Cheng, G. H. Lee, C. M. Jiang and P. T. Chou, *Inorg. Chem.*, 2007, **46**, 11202; (c) W. Lu, Y. Chen, V. A. L. Roy, S. S. Y. Chui and C. M. Che, *Coorg. Chem., Int. Ed.*, 2009, **48**, 7621; (d) A. Y. Y. Tam, K. M. C. Wong and V. W. W. Yam, *J. Am. Chem. Soc.*, 2009, **131**, 6253.
- (a) I. Eryazici, C. N. Moorefield and G. R. Newkome, *Chem. Rev.*, 2008, **108**, 1834; (b) F. Camerel, R. Ziessel, B. Donnio, C. Bourgogne, D. Guillon, M. Schmutz, C. Iacovita and J. P. Bucher, *Angew. Chem., Int. Ed.*, 2007, **46**, 2659.
- (a) B. P. Yan, C. C. Cheung, S. C. Kui, H. F. Xiang, V. A. Roy, S. J. Xu and C. M. Che, *Adv. Mater.*, 2007, **19**, 3599; (b) J. Kavitha, S. Y. Chang, Y. Chi, J. K. Yu, Y. H. Hu, P. T. Chou, S. M. Peng, G. H. Lee, Y. T. Tao, C. H. Chien and A. J. Carty, *Adv. Funct. Mater.*, 2005, **15**, 223; (c) M. A. Baldo, D. F. O'Brien, Y. You, A. Shoustikov, S. Sibley, M. E. Thompson and S. R. Forrest, *Nature*, 1998, **395**, 151; (d) G. J. Zhou, Q. Wang, C. L. Ho, W. Y. Wong, D. G. Ma and L. X. Wang, *Chem. Commun.*, 2009, 3574; (e) G. J. Zhou, W. Y. Wong and S. Suo, *J. Photochem. Photobiol.*, 2010, **11**, 133.
- (a) S. B. Zhao, T. McCormick and S. Wang, *Inorg. Chem.*, 2007, **46**, 10965; (b) N. M. Shavaleev, H. Adams, J. Best, R. Edge, S. Navaratnam and J. A. Weinstein, *Inorg. Chem.*, 2006, **45**, 9410.
- (a) M. D. Perez, P. I. Djurovich, A. Hassan, G. Y. Cheng, T. J. Stewart, K. Aznavour, R. Bau and M. E. Thompson, *Chem. Commun.*, 2009, 4215; (b) Y. Ji, R. Zhang, X. B. Du, J. L. Zuo and X. Z. You, *Dalton Trans.*, 2008, 2578; (c) Q. Zhao, F. Y. Li and C. H. Huang, *Chem. Soc. Rev.*, 2010, **39**, 3007; (d) X. Mou, S. J. Liu, C. L. Dai, T. C. Ma, Q. Zhao, Q. D. Ling and W. Huang, *Sci. China Chem.*, 2010, **53**, 1235.
- (a) D. L. Ma, C. M. Che and S. C. Yan, *J. Am. Chem. Soc.*, 2009, **131**, 1835; (b) P. K. Siu, D. L. Ma and C. M. Che, *Chem. Commun.*, 2005, 1025.
- (a) B. L. Yin, F. Niemeyer, J. A. Williams, J. Jiang, A. Boucekine, L. Toupet, B. H. Le and V. Guerschais, *Inorg. Chem.*, 2006, **45**, 8584; (b) C. A. Craig, F. O. Garces, R. J. Watts, R. Palmans and A. J. Frank, *Coord. Chem. Rev.*, 1990, **97**, 193; (c) Y. Kunugi, K. R. Mann, L. L. Miller and C. L. Exstrom, *J. Am. Chem. Soc.*, 1998, **120**, 589; (d) G. J. Zhou, C. L. Ho, W. Y. Wong, Q. Wang, D. G. Ma, L. X. Wang, Z. Y. Lin, T. B. Marder and A. Beeby, *Adv. Funct. Mater.*, 2008, **18**, 499; (e) G. J. Zhou, Q. Wang, X. Z. Wang, C. L. Ho, W. Y. Wong, D. G. Ma, L. X. Wang and Z. Y. Lin, *J. Mater. Chem.*, 2010, **20**, 7472; (f) G. J. Zhou, X. Z. Wang, W. Y. Wong, X. M. Yu, H. S. Kwok and Z. Y. Lin, *J. Organomet. Chem.*, 2007, **692**, 3461; (g) C. L. Ho, W. Y. Wong, B. Yao, Z. Y. Xie, L. X. Wang and Z. Y. Lin, *J. Organomet. Chem.*, 2009, **694**, 2735.
- (a) P. I. Kvam, M. V. Puzyk, K. P. Balashev and J. Songstad, *Acta Chem. Scand.*, 1995, **49**, 335; (b) K. P. Balashev, M. V. Puzyk, V. S. Kotlyar and M. V. Kulikova, *Coord. Chem. Rev.*, 1997, **159**, 109.
- M. Ghedini, T. Pugliese, D. M. La, N. Godbert, I. Aiello, M. Amati, S. Belviso, F. Lejl, G. Accorsi and F. Barigelletti, *Dalton Trans.*, 2008, 4303.
- (a) C. H. Shin, J. O. Huh, S. J. Baek, S. K. Kim, M. H. Lee and Y. Do, *Eur. J. Inorg. Chem.*, 2010, 3642; (b) A. Valore, A. Colombo, C. Dragonetti, S. Righettoa, D. Roberto, R. Ugoa, F. D. Angelis and S. Fantacci, *Chem. Commun.*, 2010, **46**, 2414; (c) J. Liu, C. J. Yang, Q. Y. Cao, M. Xu, J. Wang, H. N. Peng, W. F. Tan, X. X. Lü and X. C. Gao, *Inorg. Chim. Acta*, 2009, **362**, 575.
- (a) Z. Q. Chen, Z. Q. Bian and C. H. Huang, *Adv. Mater.*, 2010, **22**, 1534; (b) Q. Zhao, F. Y. Li and C. H. Huang, *Chem. Soc. Rev.*, 2011, **40**, 2508; (c) M. X. Yu, Q. Zhao, L. X. Shi, F. Y. Li, Z. G. Zhou, H. Yang, T. Yi and C. H. Huang, *Chem. Commun.*, 2008, 2115; (d) Q. Zhao, M. X. Yu, L. X. Shi, S. J. Liu, C. Y. Li, M. Shi, Z. G. Zhou, C. H. Huang and F. Y. Li, *Organometallics*, 2010, **29**, 1085; (e) H. Z. Wu, T. S. Yang, Q. Zhao, J. Zhou, C. Y. Li and F. Y. Li, *Dalton Trans.*, 2011, **40**, 1969; (f) L. Q. Xiong, Q. Zhao, H. L. Chen, Y. B. Wu, Z. H. Dong, Z. G. Zhou and F. Y. Li, *Inorg. Chem.*, 2010, **49**, 6402; (g) S. P. Y. Li, H. W. Liu, K. Y. Zhang and K. K. W. Lo, *Chem.-Eur. J.*, 2010, **16**, 8329; (h) K. Y. Zhang, H. W. Liu, T. H. Fong, X. G. Chen and K. K. W. Lo, *Inorg. Chem.*, 2010, **49**, 5432; (i) K. Y. Zhang and K. K. W. Lo, *Inorg. Chem.*, 2009, **48**, 6011; (j) T. S. Yang, A. Xia, Q. Liu, M. Shi, H. Z. Wu, L. Q. Xiong, C. H. Huang and F. Y. Li, *J. Mater. Chem.*, 2011, **21**, 5360.
- S. W. Botchway, M. Charnley, J. W. Haycock, A. W. Parker, D. L. Rochester, J. A. Weinstein and J. A. G. Williams, *Proc. Natl. Acad. Sci. U. S. A.*, 2008, **105**, 16071.
- (a) P. Wu, E. L. M. Wong, D. L. Ma, G. S. M. Tong, K. M. Ng and C. M. Che, *Chem.-Eur. J.*, 2009, **15**, 3652; (b) C. K. Koo, K. L. Wong, C. W. Y. Man, Y. W. Lam, L. K. Y. So, H. L. Tam, S. W. Tsao, K. W. Cheah, K. C. Lau, Y. Y. Yang, J. C. Chen and M. H. W. Lam, *Inorg. Chem.*, 2009, **48**, 872; (c) C. K. Koo, K. Y. Leo, K. L. Wong, Y. M. Ho, Y. W. Lam, M. H. W. Lam, K. W. Cheah, C. W. Cheng and W. M. Kwok, *Chem.-Eur. J.*, 2010, **16**, 3942.
- C. F. Wu, B. Bull, K. Christensen and J. McNeill, *Angew. Chem., Int. Ed.*, 2009, **48**, 2741.
- (a) W. J. Xu, S. J. Liu, X. Y. Zhao, S. Sun, S. Cheng, T. C. Ma, H. B. Sun, Q. Zhao and W. Huang, *Chem.-Eur. J.*, 2010, **16**, 7125; (b) K. A. King, P. J. Spellane and R. J. Watts, *J. Am. Chem. Soc.*, 1985, **107**, 1431; (c) S. Lamansky, P. Djurovich, D. Murphy, F. AbdelRazzaq, R. Kwong, I. Tsyba, M. Bortz, B. Mui, R. Bau and M. E. Thompson, *Inorg. Chem.*, 2001, **40**, 1704.
- J. DePriest, G. Y. Zheng, N. Goswami, D. M. Eichhorn, C. Woods and D. P. Rillema, *Inorg. Chem.*, 2000, **39**, 1955.
- M. J. Frisch, G. W. Trucks, H. B. Schlegel, G. E. Scuseria, M. A. Robb, J. R. Cheeseman, J. A. Montgomery, J. T. Vreven, K. N. Kudin, J. C. Burant, J. M. Millam, S. S. Iyengar, J. Tomasi, V. Barone, B. Mennucci, M. Cossi, G. Scalmani, N. Rega, G. A. Petersson, H. Nakatsuji, M. Hada, M. Ehara, K. Toyota, R. Fukuda, J. Hasegawa, M. Ishida, T. Nakajima, Y. Honda, O. Kitao, H. Nakai, M. Klene, X. L. J. E. Knox, H. P. Hratchian, J. B. Cross, V. Bakken, C. Adamo, J. Jaramillo, R. Gomperts, R. E. Stratmann, O. Yazyev, A. J. Austin, R. Cammi, C. Pomelli, J. Ochterski, P. Y. Ayala, K. Morokuma, G. A. Voth, P. Salvador, J. J. Dannenberg, V. G. Zakrzewski, S. Dapprich, A. D. Daniels, M. C. Strain, O. Farkas, D. K. Malick, A. D. Rabuck, K. Raghavachari, J. B. Foresman, J. V. Ortiz, Q. Cui, A. G. Baboul, S. Clifford, J. Cioslowski, B. B. Stefanov, G. Liu, A. Liashenko, P. Piskorz, R. L. I. Komaromi, D. J. Fox, T. Keith, M. A. A. Laham, C. Y. Peng, A. Nanayakkara, M. Challacombe, P. M. W. Gill, B. G. Johnson, W. Chen, M. W. Wong, C. Gonzalez and J. A. Pople, *GAUSSIAN 03*, Gaussian, Inc., Wallingford, CT, 2004.
- (a) B. Delley, *J. Chem. Phys.*, 2000, **113**, 7756; (b) B. Delley, *J. Chem. Phys.*, 1990, **92**, 508; (c) J. P. Perdew, K. Burke and M. Ernzerhof, *Phys. Rev. Lett.*, 1996, **77**, 3865.
- B. Delley, *Phys. Rev. B: Condens. Matter*, 2002, **66**, 155125.
- G. M. heldrick, *SHELXTL-97, A Program for Crystal Structure Refinement*; Universität of Göttingen: Germany, 1997.
- (a) K. Zhang, Z. Y. Chen, Zou, C. Yang, J. G. Qin and Y. Cao, *Organometallics*, 2007, **26**, 3699; (b) S. A. Fuqua and R. M. Silverstein, *J. Org. Chem.*, 1964, **29**, 395.

- 23 (a) K. K. W. Lo, K. H. K. Tsang and N. Zhu, *Organometallics*, 2006, **25**, 3220; (b) K. K. W. Lo, P. K. Lee and J. S. Y. Lau, *Organometallics*, 2008, **27**, 2998.
- 24 Z. Cheng, A. K. Chen, H. Y. Lee and A. Tsourkas, *Drug. Deliv.*, 2010, **6**, 1398.
- 25 C. M. Laurent, Y. Z. Edgar and Alexander, *Inorg. Chem.*, 1984, **23**, 4249.
- 26 (a) T. Johansson, W. Mammo, M. Svensson, M. R. Andersson and O. Inganäs, *J. Mater. Chem.*, 2003, **13**, 1316; (b) S. L. Michelle, J. Luo and A. K. Y. Jen, *Chem. Mater.*, 2003, **15**, 3496.
- 27 H. Jude, J. A. K. Bauer and W. B. Connick, *J. Am. Chem. Soc.*, 2003, **125**, 3446.
- 28 (a) C. C. Deuschel and A. V. Zelewsky, *Inorg. Chem.*, 1987, **26**, 3354; (b) M. V. Kulikova, K. P. Balashev, P. I. Kvam and J. Songstad, *Russ. J. Gen. Chem.*, 2000, **70**, 163.
- 29 K. K. Lo, D. C. Ng and C. K. Chung, *Organometallics*, 2001, **20**, 4999.
- 30 (a) G. A. Crosby, *Acc. Chem. Res.*, 1975, **8**, 231; (b) W. Lu, B. X. Mi, M. C. Chan, Z. Hui, C. M. Che, N. Y. Zhu and S. T. Lee, *J. Am. Chem. Soc.*, 2004, **126**, 4958.
- 31 (a) F. Neve, D. M. La, A. Crispini, A. Bellusci, F. Puntoriero and S. Campagna, *Organometallics*, 2004, **23**, 5856; (b) M. Lepeltier, T. K. Lee, K. K. Lo, L. Toupet, B. H. Le and W. Guerschais, *Eur. J. Inorg. Chem.*, 2005, 110.
- 32 (a) J. S. Field, L. P. Ledwaba, O. Q. Munro and D. R. McMillin, *CrystEngComm*, 2008, **10**, 740; (b) Y. Sun, K. Ye, H. Zhang, J. Zhang, L. Zhao, B. Li, G. Yang, B. Yang, Y. Wang, S. W. Lai and C. M. Che, *Angew. Chem., Int. Ed.*, 2006, **45**, 5610; (c) V. W. W. Yam, K. H. Y. Chan, K. M. C. Wong and N. Zhu, *Chem.–Eur. J.*, 2005, **11**, 4535.